Macromolecular Materials and Engineering
Open Access
www.mame-journal.de

A Novel Strategy as a Potential Rapid Therapy Modality in the Treatment of Corneal Ulcers: Fluconazole/Vancomycin Dual Drug-Loaded Nanofibrous Patches

Sumeyye Cesur, Elif Ilhan, Esra Pilavci, Rabia Betul Sulutas, Merve Gurboga, Ozlem Bingol Ozakpinar, Elif Kaya, Marcin Heljak, Gulgun Bosgelmez Tinaz, Faik Nuzhet Oktar, Oguzhan Gunduz, and Ewa Kijeńska-Gawrońska**

Corneal ulcer, which is brought on by a breach in the epithelial barrier, is a dangerous infection of the avascular corneal stroma. New treatment strategies are needed, suppressing the aggressive nature of the disease and including a combination of different drugs. In this study, vancomycin (VAN) and fluconazole (FLU) dual-drug loaded dual-layered polyvinyl alcohol and gelatin (PVA/GEL) nanofibrous patches are produced by electrospinning. Scanning electron microscopy (SEM) images show smooth surfaces are obtained for both pure and drug-loaded nanofibrous patches. The tensile test results report that loading the FLU and VAN separately into the PVA/GEL patches decrease both the tensile strength and elongation at break and it is further reduced when combining two drug-loaded layers in one patch. According to drug release results, the FLU and VAN-loaded nanofibrous patches show a controlled release profile extending up to 96 h. Moreover, PVA/GEL/FLU, PVA/GEL/VAN, and PVA/GEL/FLU/VAN nanofibrous patches display significant antimicrobial activity against *Candida albicans* and *Staphylococcus aureus*. SEM, 4'-6diamidynofenyloindol (DAPI) staining, and 3-(4,5-dimethylthiazol-2-yl)-2,5-diphenyltetrazolium bromide (MTT) assay show that PVA/FLU and PVA/GEL/FLU/VAN nanofibrous patches have a superior effect on NIH3T3 cell spreading and proliferation. The novelty of this study lays in the development of a potential dual drug rapid treatment for corneal ulcers of aggressive nature.

1. Introduction

The cornea, located in the front area of the iris and pupil, is the part that refracts the light reaching the eye and transmits it to the retina and protects the eye from external factors. The layers of the cornea, which are physiologically avascular and transparent, consist of epithelium with self-renewal properties and a stromal that maintains transparency.[1] The layered organization of collagen fibers and the extracellular matrix (ECM) supports the cornea in terms of shape and integrity. The cornea of an adult human eye has a horizontal diameter of ≈11.5 mm and a vertical diameter of 10.5 mm, and displays a constant curvature throughout life.[2]

A corneal ulcer is a crucial ocular injury that threatens vision due to the defect in the corneal epithelium. Corneal ulcer requiring urgent treatment is a risky health problem that can lead to vision loss. Complications such as corneal scarring and perfusion, glaucoma development, cataract, and eye synechia, known as the destruction of the visual nerves by the pressure

S. Cesur, E. Ilhan, E. Pilavci, R. B. Sulutas, F. N. Oktar, O. Gunduz
Center for Nanotechnology & Biomaterials Application and Research (NBUAM)
Marmara University
Istanbul 34722, Turkey
E-mail: sumeyye.cesur@marmara.edu.tr

The ORCID identification number(s) for the author(s) of this article can be found under https://doi.org/10.1002/mame.202200697

DOI: 10.1002/mame.202200697

S. Cesur, E. Pilavci, R. B. Sulutas, O. Gunduz
Department of Metallurgical and Materials Engineering, Faculty of Technology
Marmara University
Istanbul 34722, Turkey

E. Ilhan, F. N. Oktar
Department of Bioengineering, Faculty of Engineering
Marmara University
Istanbul 34854, Turkey

M. Gurboga, O. Bingol Ozakpinar
Department of Biochemistry, Faculty of Pharmacy
Marmara University
Istanbul 34668, Turkey

E. Kaya, G. Bosgelmez Tinaz
Department of Basic Pharmaceutical Sciences, Faculty of Pharmacy
Marmara University
Istanbul 34668, Turkey

inside the eye, trigger morbidity.[3] It has been stated that corneal transplants for the treatment of infectious keratitis constitute a small portion of ≈12.2% of all transplants. Therefore, this problem should be recognized and detected quickly in order to initiate emergency treatment and intervene when the disease is still at a preventable level.[4] Corneal ulcers are caused by bacterial, viral, fungal, protozoan, and autoimmune diseases. The most common etiology is bacterial pathogens. The onset of corneal ulcers occurs with the formation of keratitis (corneal inflammation) by the bacteria entering that area due to the break in the corneal epithelium, which is the protective layer. The reasons for the fractures in the corneal epithelium are commonly contact lens wear, corneal abrasion, ocular traumas, and rarely a history of diabetes, chronic ocular disease, use of corticosteroid drugs, and agricultural work. *Staphylococcus aureus (S. aureus)* and *Pseudomonas aeruginosa* (*P. aeruginosa*) are the most common bacterial pathogens. *Staphylococcus epidermidis* (*S. epidermidis*) and *Staphylococcus fusarium* (*S. fusarium*), the most common species in polymicrobial keratitis, trigger ocular trauma. *Aspergillus, Fusarium, Candida albicans* (*C. albicans*), and other Candida species are fungal species that cause corneal infections. Acanthamoeba, a free-living protozoan, is classified as a corneal ulcer-causing protozoan, and is found in freshwater sources and soil.[5]

The use of anti-infective drugs for the treatment of corneal ulcers is the most commonly utilized medical solution.[6] Fluconazole (FLU) is a widely used bistriazole fungistatic agent with high efficacy and low toxicity. FLU, treats keratitis with deep lesions in intraocular applications thanks to its penetrating property. It has been proven that that FLU works against gram-positive bacteria in disease states, where natamycin and miconazole are insufficient.[7] Some of the antimicrobial drugs applied in the clinical treatment of corneal keratitis show weak cleavage in the corneal mucus layer. In addition, low ocular bioavailability has been a limiting problem for conventional eye drops due to the inability to reach the desired therapeutic dose caused by the short residence time in the eye. This situation requires the use of high doses of drugs, which causes the drug to enter circulation systematically and increases the side effects. Compared to conventional clinical eye drops, controlled drug delivery assays such as nanofibers are highly demanded.[8]The study of Yehgambaram et al. proved that FLU loaded polyaniline (PANI) has high antifungal properties by testing it on *C. albicans, C. tropicalis,* and *C. krusei* strains.[9] Sharma et al. have shown that the pharmaceutical carrier system in which polyvinyl alcohol (PVA) nanofibrous patch and FLU are used together for the treatment of vaginal candidiasis, has superior antifungal activity potential compared to drug-free systems.[10]

M. Heljak, E. Kijeńska-Gawrońska
Faculty of Materials Science and Engineering
Warsaw University of Technology
Warsaw 02-507, Poland
E-mail: ewa.kijenska@pw.edu.pl
E. Kijeńska-Gawrońska
Centre for Advanced Materials and Technologies CEZAMAT
Warsaw University of Technology
Warsaw 02-822, Poland

Vancomycin (VAN) is a glycopeptide antibiotic that inhibits the synthesis of the cell wall in Gram-positive microorganisms.[11] Its mechanism is the inhibition of the peptidoglycan synthesis pathway within the microorganism cell wall. Furthermore, it has restricted antimicrobial activity against gram-negative bacteria because of the molecular size-exclusion impact on the microorganism's outer membrane.[12] It has been a useful therapeutic option in treating bacterial-infected corneal ulcers.[13] In a study, Naeimi et al. reported that VAN-loaded CS/PVA/Polyethylene glycol (PEG) hydrogel wound dressing had antimicrobial activity.[14] In another study, a VAN-loaded injectable nanofibrous hydrogel patch showed good antimicrobial and biocompatible properties.[15] In the study by Riau et al., VAN-loaded collagen hydrogel exhibited a good drug release profile. The hydrogel was implanted in vivo in a rabbit model with keratitis and reduced the infection.[16] However, the performance of VAN is limited by the lack of its oral absorption. The infusion time should not be less than 1 h, as rapid intravenous infusion may cause skin reactions.[17] Nanofibrous patches have a large specific surface area that can stabilize drugs.[18]

Electrospinning allows producing nanometer-scale fibers. Its cardinal working mechanism is the electrophysical interplay between the electrostatic force and the polymer solution.[19] The nanofibrous patch consists of pores and fibers with a large surface area that also allows cell adhesion and proliferation. The most spectacular advantage of electrospinning is that obtained nanofibrous patches can prolong the release of drugs compared with solution form. In this method, drugs can be incorporated into the nanofibrous patch by blending the drug and the polymer solution.[20] Various natural and synthetic polymers and their rational combinations are used in drug delivery systems with electrospinning.[21]

PVA is a synthetic polymer frequently used in many tissue engineering applications, such as treating corneal diseases. Due to its properties like biodegradability, biocompatibility,[22] hydrophilicity,[23] good flexibility, good oxygen permeability, and high drug loading potential, it is widely used in artificial blood vessels, dressing studies, and contact lenses.[24] Miyashita et al. reported that the PVA-Collagen scaffold that they produced was compatible with the corneal epithelium due to its high oxygen permeability feature.[25] For the treatment of corneal ulcers, bacterial keratitis, and other corneal infectious diseases, Jain et al. loaded ciprofloxacin in PVA/Gel mixes using the solution casting method. They demonstrated that PVA/gelatin blends are preferable to conventional eye drops for the controlled release of antibiotics in the eye.[26] In a different investigation by Huang et al., they compared randomly oriented and aligned PVA/Gel nanofibers and discovered that cells on the PVA-gelatin aligned fibers widely spread out.[27] In another study, PVA/GEL-based propolis-loaded nanofibrous patches were used to treat microbial keratitis.[28]

Presented investigation aimed to produce dual-layered PVA/GEL nanofibrous patches loaded with two drugs (FLU and VAN) by electrospinning and to assess their biological efficacy. The in vitro antifungal and antibacterial activities of FLU and VAN-loaded PVA/GEL nanofibrous patches against *C. albicans* and *S. aureus* were evaluated. Additionally, we have determined the in vitro cytotoxic effects and wound healing activity. The novelty of this study is to develop a potential rapid treatment

Table 1. Components and proportions in all nanofibrous patches produced.

Nanofibrous patches	PVA content [wt%]	GEL content [wt%]	Tween 80 [wt%]	Drug amount [wt%]
PVA/GEL	13	0.5	3	—
PVA/GEL/FLU	13	0.5	3	0.2
PVA/GEL/VAN	13	0.5	3	5
PVA/GEL/FLU/VAN	13	0.5	3	0.2+5

modality for the treatment of corneal ulcers of aggressive nature with dual drug therapy.

2. Experimental Section

2.1. Materials

Gelatine from bovine skin (powder, gel strength ≈225 g bloom, Type B), Poly (vinyl alcohol) with Mw of about 89 000–98 000 (99+% hydrolyzed), Tween 80 (viscous liquid), phosphate buffer saline (PBS, pH = 7.4), and Glutaraldehyde solution (GA, 50 wt%, $M_W = 100.12$ g mol^{-1}) were purchased from Sigma-Aldrich (St. Louis, MO). FLU ($M_W = 306.27$ g mol^{-1}) and VAN ($M_W = 1449.25$ g mol^{-1} (free base basis)) were purchased from Sigma-Aldrich, Darmstadt, Germany.

2.2. Method

2.2.1. Preparation of the Solutions for Electrospinning of Nanofibrous Patches

Solutions containing different amounts of drug were prepared as states in the **Table 1**. 13 wt% PVA solution was prepared in DI water by stirring in a magnetic stirrer (Wise Stir, MSH-20 Germany) for 1 h at 650 rpm and 90 °C. The surfactant Tween 80, 3 wt% was added dropwise into the dissolved PVA and mixed for 15 min at 800 rpm at room temperature. Then, 0.5 wt% of gelatine powder was added to the solution and the solution was further stirred at 650 rpm for 15 min at 60 °C. 0.2 wt% FLU and 5 wt% VAN drugs were added to the prepared solution separately and mixed at 200 rpm for 30 min.

2.2.2. Preparation Stage and the Optimization Parameters of the Electrospinning Process

A laboratory scale device (NS24, Inovenso Co., Turkey) was used to perform electrospinning and to collect the fibrous layers with uniform thickness. The electrospinning process for each type of solution was optimized. The syringe containing the solution was placed in the pump. The required flow rate from the pump connected to the power source has been set at 0.5 mL h^{-1}. To collect the nanofibrous patches, a cylindrical collector with a rotating head was placed at a distance of 12 cm from the metal floor to which the needles were fixed. The system was set up by wrapping wax paper around the collector. The waxed paper was weighed before the process. Electrospinning was performed at 25 kV, and for a total of 7 h. Drug-loaded solutions containing 0.2 wt% FLU and 5 wt% VAN were produced separately for 7 h. For additive production, 0.2 wt% FLU loaded solution was electrospun for 3 h and 30 min. Afterward, the syringe and solution were changed and PVA/GEL solution with 5 wt% VAN was electrospun for next 3 h and 30 min. This way, a combination fiber assembly containing two different drug-loaded layers was obtained. After electrospinning each waxed paper with collected fibers were weighed and its weight was recorded. Layered fiber combination, created by loading the two drugs into separate layers, was labeled as PVA/GEL/FLU/VAN, and the mechanism of its production has been shown in **Figure 1**.

2.2.3. Crosslinking Process

Nanofibrous patches were crosslinked with glutaraldehyde vapors. For this, the nanofibrous patches were placed inside the desiccator over the glutaraldehyde solution and incubated at 40 °C for 5 h in an oven.

2.2.4. Morphology and Porosity Characterization of the Nanofibrous Patches

SEM (EVO LS 10, Zeiss) was used to examine the surface morphologies of nanofibrous patches. First, the surface of drug-loaded and nondrug-loaded fibers was coated with a layer of gold and palladium for 120 s with a spray coating machine (Quorum SC7620, USA). Further, according to the obtained SEM results, histogram graphs were drawn by taking measurements of 100 fiber using imaging software (Olympus AnalySIS, USA).

Porosity of the investigated nanofibrous patches was determined based on SEM images using CTAn software (Bruker, Belgium).

Nanofibrous patches' thickness was measured using the micrometer screw gauge. Data were expressed as mean ± standard deviation ($n = 3$).

2.2.5. Chemical Properties Characterization of the Nanofibrous Patches Using Fourier-transformed infrared spectroscopy (FTIR)

FTIR (Jasco FT/IR-4700 model machine) was used to analyze the chemical structures and functional groups of nanofibrous patches. The spectra were recorded performed in transmission mode at a scanning range of 4000–400 cm^{-1} at a resolution of 4 cm^{-1} and a scanning speed of 32 at room temperature (23 °C).

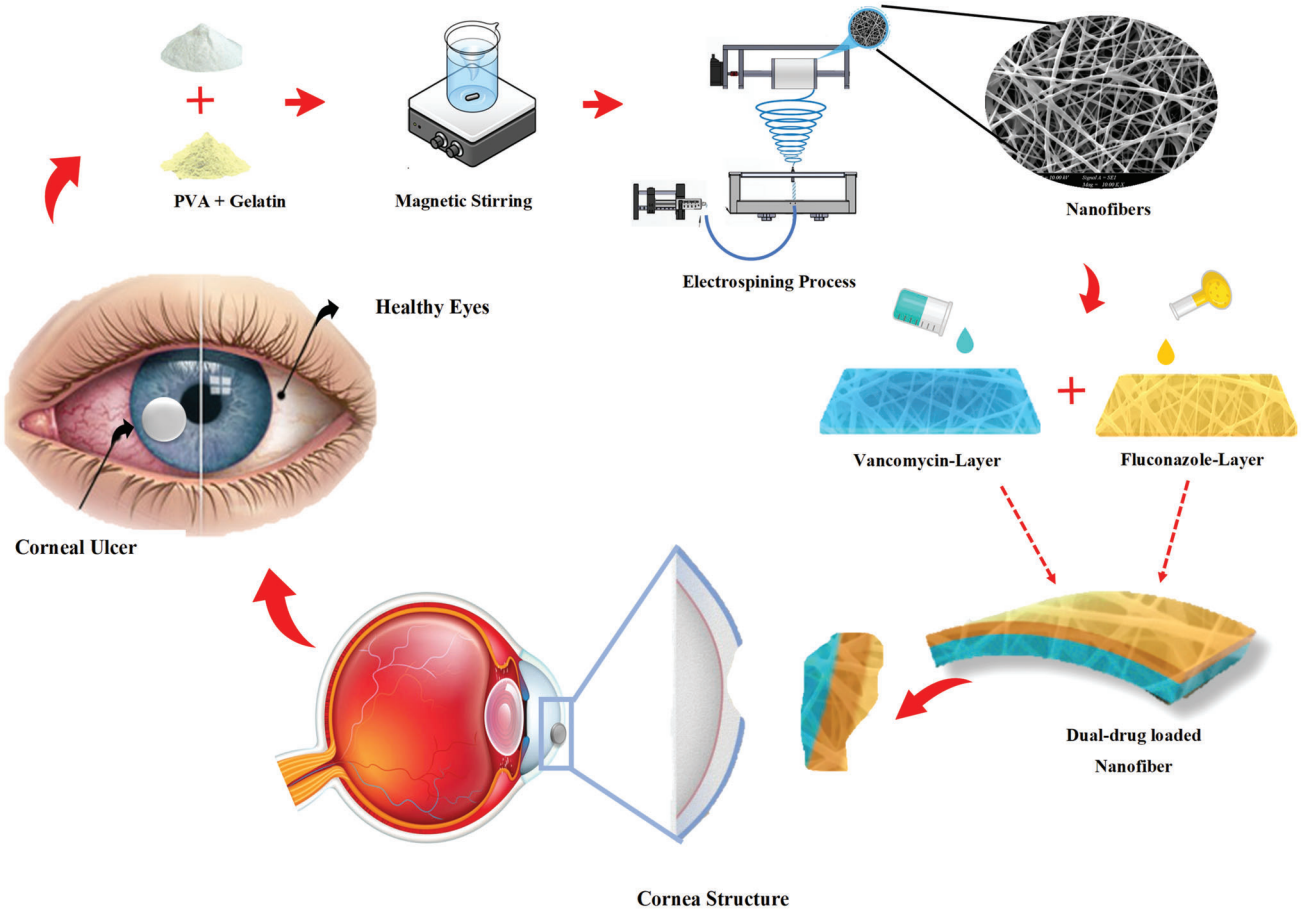

Figure 1. Schematic illustration of the production of dual drug-loaded nanofibrous patches for corneal ulcers treatment.

2.2.6. Thermal Properties Characterization of the Nanofibrous Patches Using DSC

Glass transition temperature (T_g) and melting temperature (T_m) of nanofibrous patches were analyzed using differential scanning calorimetry (DSC) (Shimadzu, Japan). To measure the changing behavior of the material under thermal conditions, nanofibrous patches were processed in the DSC device between 25 and 300 °C and 10^0 heating rate.

2.2.7. Properties of Nanofibrous Patches

A tensile testing machine (Shimadzu Corporation, EZ-LX, Kyoto, Japan) was used to analyze the nanofibrous patches' mechanical properties. Before the tensile test, the thickness of the nanofibrous patches was calculated using a digital micrometer (Mitutoyo MTI Corp., USA) and dimensions of the samples were adjusted to 10 × 50 mm. For each group, three different samples were tested.

2.2.8. Swelling and Degradation Behaviors of Nanofibrous Patches

Swelling and degradation measurements were taken in order to determine the water-taking capacity of the nanofibrous patches, and the changes in their mass with time. Phosphate buffered saline (PBS) with a pH of 7.4 was used for the swelling tests. During this tests, the initial weights of the nanofibrous patches of equal weight were recorded. The nanofibrous patches were then transferred into Eppendorf tubes containing 1 mL of PBS and kept at 37 °C in a thermal shaker (BIOSAN TS-100). After 24 h, the samples were removed from the excess water and their wet weights were measured. Equation (1) was used to measure the swelling value[29]

$$S = \frac{Ww - Wo}{Wo} \times 100 \quad (1)$$

Nanofibrous patches were weighed equally for the degradation process and placed in a thermal shaker device in PBS in 1 mL Eppendorf tubes. After 1 day, the samples and PBS were separated from each other and the fibers were dried in the thermal heater for 24 h. The degradation calculation of nanofibrous patches whose weights were measured after drying (Wt) was made according to Equation (2)[30]

$$D = \frac{Wo - Wt}{Wo} \times 100 \quad (2)$$

2.2.9. Efficiency, In Vitro Drug Release, and Drug Release Kinetics

The encapsulation efficiency (%EE) was investigated to measure the amount of drug-loading capacity of the nanofibrous patches using a UV–VIS spectrophotometer (Shimadzu UV-3600, Kyoto, Japan). 10 mg of nanofibrous patches was completely dissolved in a solvent by mixing. From each solution, 1 mL was taken and evaluated using a spectrophotometer. All measurements were performed in triplicates. The %EE was calculated by the following Equation (3)

$$\text{Encapsulation efficieny} = \frac{\text{mass of actual drug loaded in nanofibers}}{\text{mass of used in nanofiber fabrication}} \times 100 \quad (3)$$

For the in vitro release study in PBS (7.4 pH). 5 mg of nanofibrous patch was added to 1 mL of PBS at 37 °C and kept in a thermal shaker (BIOSAN TS-100, Riga, Latvia). Measurements were taken with UV spectrophotometer at certain time intervals. Every time 1 mL was replaced with fresh PBS to continue the release studies.

The zero-order, first-order, Korsmeyer–Peppas, Higuchi, and Hixson–Crowell models mathematical models were used to evaluate the drug release

$$Q = Kt^n \quad (4)$$

$$Q = K_0 t \quad (5)$$

$$In\left(1 - Q\right) = -K_1 t \quad (6)$$

$$Q = K_h t^{1/2} \quad (7)$$

$$Q^{1/3} = K_{hc} t \quad (8)$$

In these equations, Q is the fractional amount of drug release at time t; K_0, K_1, K, K_h, and K_{hc} are the kinetic constants for zero-order, first-order, Korsmeyer–Peppas Higuchi, and Hixson–Crowell models, respectively. "n" is the diffusion exponent, which is indicative of the drug release mechanism.

2.2.10. Activity of PVA/GEL/FLU and PVA/GEL/FLU/VAN Nanofibrous Patches

Antifungal Activity Assay: The antifungal activity of PVA/GEL/FLU and PVA/GEL/FLU/VAN nanofibrous patches was tested using the disc diffusion method as described by the Clinical Laboratory Standards Institute (CLSI) (1). *C. albicans* (ATCC 90023) was used as reference strain. *C. albicans* was grown in Sabouraud dextrose agar (SDA) for 48 h at 37 °C. After 48 h, turbidity of the yeast suspension was adjusted to the McFarland 0.5 cfu mL^{-1} and spread onto Mueller–Hinton Agar (MHA) plates supplemented with 2% Glucose and 0.5 µg mL^{-1} Methylene Blue Dye Medium (GMB) using a sterile cotton swab. PVA/GEL/FLU/VAN nanofibrous patches were cut into 6 mm discs and placed on the MHA plates and incubated at 37 °C for 24 h. The zone of inhibition around discs were determined by measuring the zone diameters using a ruler.

Antibacterial Activity Assay: The antibacterial activity of PVA/GEL/VAN and PVA/GEL/FLU/VAN nanofibrous patches was tested by disc diffusion method (Kirby–Bauer method). *Staphylococcus aureus* (*S. aureus)* ATCC 25923 was grown in Mueller–Hinton broth (Merck, Germany) overnight at 37 °C. The turbidity of the culture was adjusted to 0.5 McFarland standard and spread onto Mueller–Hinton Agar plates. PVA/GEL/VAN and PVA/GEL/FLU/VAN nanofibrous patches were cut into 6 mm discs were placed on the agar plates and incubated for 24 h at 37 °C. After incubation, the diameters of the growth inhibition zones around nanofibrous patches were measured.

2.2.11. Proliferation of Cells in Contact with Nanofibrous Patches

Mouse embryonic fibroblasts (NIH/3T3) were cultured in Dulbecco's modified eagle medium (DMEM) that contained 10% v/v fetal bovine serum (FBS) and 1% v/v penicillin-streptomycin in a humidified incubator at 37 °C with 5% CO_2. Before being cocultured with the cells, small pieces of nanofibrous patches were sterilized using ultraviolet for 30 min on each side. Then, the nanofibrous patches were transferred to the DMEM medium containing 10% FBS and 1% penicillin-streptomycin. The cytotoxicity evaluation was determined by MTT (3-(4,5-dimethylthiazol-2-yl)-2,5-diphenyl tetrazolium bromide) test (Vybrant MTT Cell Proliferation Assay Kit, Thermo Fisher Scientific). First, the NIH/3T3 cells were seeded in 96-well plates and cultured for 24 h. Next, the nanofibrous patches of different masses were added and cocultured for another 24, 96, and 168 h. In order to evaluate the proliferation of the cells cultured with contact with nanofibrous patches 10 μL MTT solution was added to the well and cultured for another 4 h, and cell viability was measured using a microplate reader (Bio-Tek ElX800; Bio-Tek U.S., Winooski, VT, USA) at the wavelength of 570 nm after adding 200 μL SDS buffer to each well in the plate. Viability was evaluated as follows: Cell Viability (%) = (OD test /OD control) x100.

2.2.12. DAPI Staining

To investigate the attachment and cell viability of fibroblast cells on FLU and VAN loaded PVA/GEL nanofibrous patches, DAPI staining method was performed. The fibroblast cells at a density of 10^5 cells mL^{-1} were seeded onto each nanofibrous patch in a 48-well plate and cultured in medium containing DMEM at 37 °C under 5% CO_2 for 1, 4, and 7 days. The samples were then washed twice with PBS and fixed with methanol for 10 min. The excess methanol was then removed by washing with PBS, and the cell nuclei were stained with 300 nM DAPI solution for 5 min at dark. Next, the nanofibrous patches were rinsed three times with PBS to remove excess DAPI and investigated using a fluorescence microscope.

2.2.13. SEM Analysis

Fibroblast cell growth and spread morphology on nanofibrous patches was investigated with SEM observation. FLU and VAN loaded PVA/GEL nanofibrous patches were washed twice with

PBS; fixed in 2.5% glutaraldehyde solution for 24 h at 4 °C. The excess glutaraldehyde was then removed by washing with PBS and nanofibrous patches were dehydrated in a graded ethanol series. The samples were sputter-coated with gold and examined using SEM (EVO MA-10, Zeiss).

2.2.14. Wound Healing

In vitro scratch wound healing assay is one of the most widely used 2D methods to determine the cellular migration and proliferation in processes such as regeneration and cancer. We seeded the NIH3T3 cells in a 6-well plate at a concentration of 5×10^5 cell per well and the cells were starved with 1% v/v FBS medium for 24 h. Cell cultures with a 200 μL sterile pipette tip were scratched and then washed away detached cells with sterile PBS. Then, the fresh medium was added and nanofibrous patches were cocultured with cells. After the incubation for 24 and 48 h, the cells around the wounds were visualized and imaged under an inverted microscope (4x objective lens; two fields of view per replicate, for two replicates). The percentages of the open wound areas were estimated under a microscope and analyzed using ImageJ program. The percentage of wound closure was calculated as follows

$$\text{Woundclosure}\,(\%) = \left(\left(A_{0\_}A_t\right)/A_0\right) \times 100 \quad (9)$$

A_0 is the initial wound area, A_t is the wound area after n hours of the initial scratch.

2.2.15. Statistical Analysis

All experiments were done in triplicates. The results were expressed as mean± SD. One-way analysis of variance (ANOVA) was used to determine the statistical differences. A p value <0.05 was considered statistically significant.

3. Result and Discussion

3.1. Morphological Characterization of Nanofibrous Patches

Surface morphologies of nanofibrous patches were investigated using SEM. Diameter measurements were taken from 100 fibers for each sample, and these values are shown in the histogram in **Figure 2**. SEM images demonstrated that nanofibrous patches with monodisperse and smooth surfaces were obtained, in both the pure and the drug-loaded versions (Figure 2). The thinnest fibers were obtained for the PVA/GEL sample, while the individual additions of FLU and VAN made the fibers thicker. The mean diameters of PVA/GEL, PVA/GEL/FLU, PVA/GEL/VAN, PVA/GEL/VAN/FLU nanofibrous patches were measured as 86.36 ± 15.338, 118.66 ± 27.542, 91.94 ± 15.194, and 230.73 ± 92.3 nm, respectively. According to these results, it can be said that there is an increase in the diameters of the drug-loaded nanofibrous patches compared to the pure ones. Yang et al. reported that loading the antibiotic Ciprofloxacin hydrochloride (CipHcl) into the chitosan (CS)/poly(vinyl alcohol)(PVA) nanomembrane caused a diameter change. The diameter of the fibers containing CS/PVA was 84.6 ± 21.4 nm, while the diameter of the fibers containing CSA/PVA/CipHcl has increased to 136.6 ± 32.9 nm.[31] Semnani et al., in their study, reported that when they added 10%, 20%, and 30% FLU to PVA nanofibers, the fiber diameters increased depending on the increasing amount of FLU.[32] Kalalinia et al., observed that there was an increase in diameter in the fibers when 2.5% and 5% VAN was added.[33]

Some morphological features, like the porosity and thickness of the fabricated nanofibrous patches, were determined. And the average porosity was 54.5 ± 0.7%, 58 ± 5.6%, 55 ± 1.4% and 56.5 ± 6.3% for PVA/GEL, PVA/GEL/FLU, PVA/GEL/VAN, and PVA/GEL/FLU/VAN, respectively. The average thickness was determined and the thickness of PVA/GEL was 41.6 ± 1.1 μm, PVA/GEL/FLU was 41.6 ± 1.5 μm, PVA/GEL/VAN was 46.0 ± 1.0 μm and 43.0 ± 1.0 μm for PVA/GEL/FLU/VAN It is worth mentioning that the determined average patches' thickness is considerably lower than those characterizing commonly used hydrogel contact lenses.[34,35]

3.2. Chemical Properties of the Nanofibrous Patches

In this study, FTIR analysis was used to characterize PVA/GEL, PVA/GEL/FLU, PVA/GEL/VAN, and PVA/GEL/FLU/VAN nanofibrous patches. For pure GEL (**Figure 3**A(a)), the appearance of absorption bands was seen as N–H bending at 1525 cm^{-1}, C–H stretching at 2933 cm^{-1}, C=O stretching at 1626 cm^{-1}, and N–H stretching at 3277 cm^{-1}.[18] For pure PVA (Figure 3A(b)), sharp bands were observed at 3268 cm^{-1} corresponding to O–H stretching, at 1646 cm^{-1} C=O and C=O stretching of the acetate groups, at 2910 cm^{-1} C–H stretching of the alkyl groups, and at 1417 cm^{-1} C–H_2 stretching.[36] In Figure 3A(c), the peak at 3200 cm^{-1} is due to the OH stretching in FLU. The presence of a peak at 1620 cm^{-1} corresponds to C–N stretching which indicates the presence of a triazole ring in FLU. Absorption bands at 1504–1619 cm^{-1} indicate the C–C stretching, and 3060 cm^{-1} means C–H stretching. Peaks at 1083 and 1112 cm^{-1} indicate the presence of C–F bonds.[37,38] In Figure 3A(d), the FTIR spectrum of the VAN showed characteristic peaks at 3277 cm^{-1} of OH^- stretch and 1626 cm^{-1} of C and O stretch, 1525 cm^{-1} of C.[39] In Figure 3B(e), the FTIR spectrum of the PVA/GEL had a nearly equal spectrum with pure PVA with a peak at 1324 cm^{-1}. With the GEL addition, it can be observed that the absorption band at 3277 cm^{-1} shifted to 3270 cm^{-1}. Figure 3B(f), presents the specific vibrations at 2919, 1417, and 917 cm^{-1} caused by the FLU addition to the fiber. Figure 3B(g) is the absorbance spectrum of the PVA/GEL/VAN. In the spectrum, VAN addition affected the absorbance spectrum of the PVA/GEL at the same points with a peak at 2915, 1419, and 838 cm^{-1}. Characteristic peaks of all of the drugs were observed in PVA/GEL/FLU/VAN fiber (Figure 3B(h)). Thus, it can be said that drug encapsulation was successfully achieved.

3.3. Thermal Properties of Nanofibrous Patches

Results of thermal measurements performed for PVA/GEL, PVA/GEL/VAN, PVA/GEL/FLU, PVA/GEL/VAN/FLU nanofibrous patches such as glass transition temperature (T_g), melting

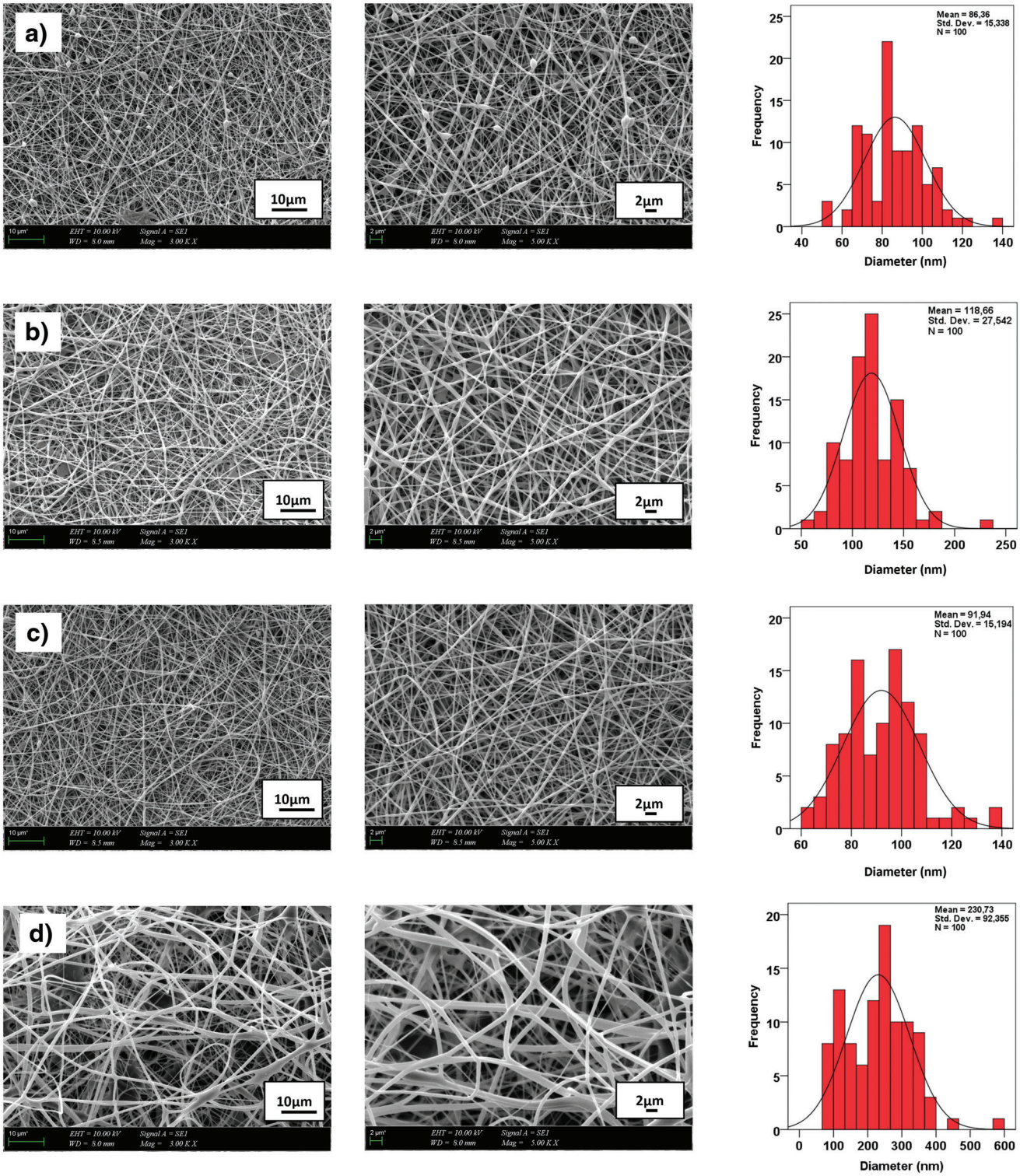

Figure 2. Morphological images of nanofibrous patches obtained by SEM and histogram graphs of diameters; PVA/GEL a), PVA/GEL/FLU b), PVA/GEL/VAN c), PVA/GEL/VAN/FLU d).

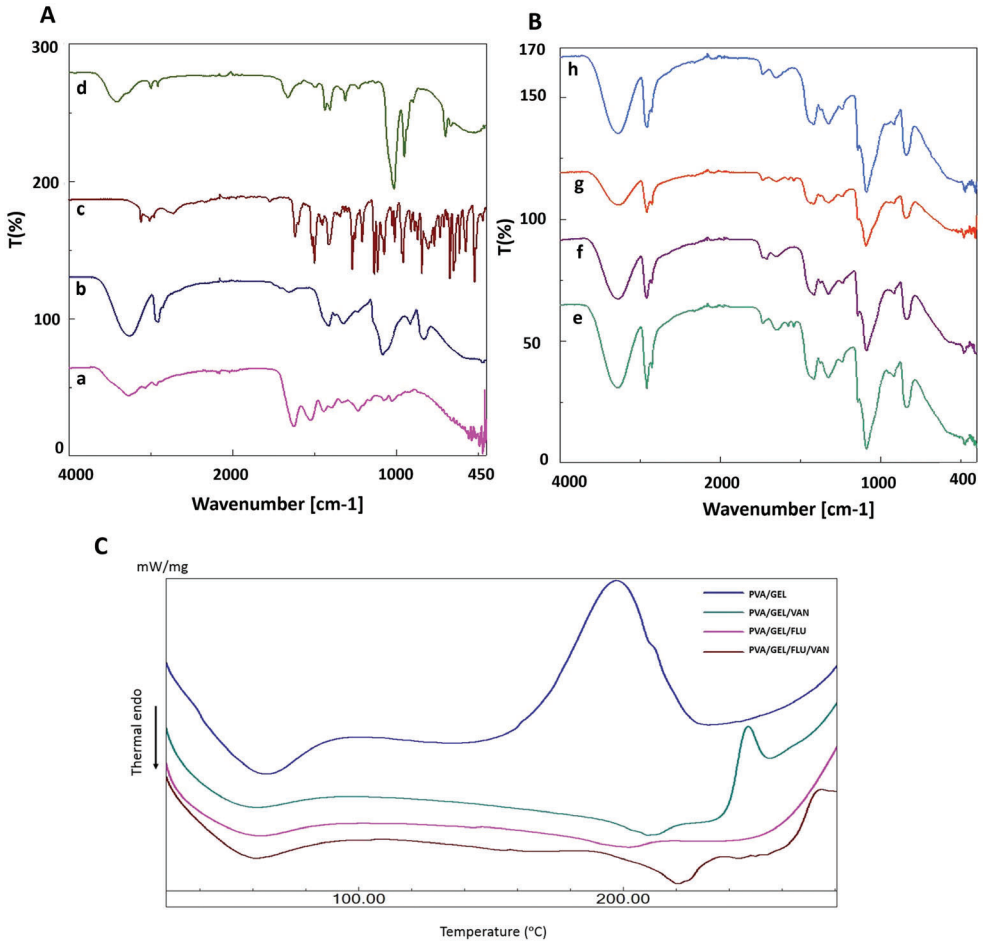

Figure 3. FTIR spectra of A) pure GEL (a), pure PVA (b), FLU (c), VAN (d), B) PVA/GEL (e), PVA/GEL/FLU (f), PVA/GEL/VAN (g), PVA/GEL/FLU/VAN (h) nanofibrous patches. C) DSC graphs of PVA/GEL, PVA/GEL/VAN, PVA/GEL/FLU, PVA/GEL/FLU/VAN nanofibrous patches.

point (T_m) are shown in Figure 3C. Linh et al., obtained melting temperature of pure PVA of 228 °C and the melting temperature of gelatine was 95.8 °C. Linh et al. found that the melting point decreases when PVA and gelatine are mixed in different proportions.[40] According to our results, the T_m of the PVA/GEL nanofibrous patch mixture also decreased to 197.24 °C. The melting temperature of PVA/GEL/VAN, PVA/GEL/FLU, PVA/GEL/VAN/FLU nanofibrous patches was 247.21, 255.03, and 274.91 °C, respectively. It was concluded that the drugs added to the PVA and gelatine solution affected the melting temperature. The glass transition temperatures of PVA/GEL, PVA/GEL/VAN, PVA/GEL/FLU, PVA/GEL/FLU/VAN are as follows: 65.22, 61.75, 57.97, and 57.99 °C. When antibiotic, and antifungal drugs were added to the nanofibrous patches, no significant change was observed in the glass transition temperature.[7] Naeimi et al., in their study, proved that there was a decrease in T_m value as the PVA ratio increased while preparing a VAN-loaded dressing.[14] Because the PVA ratio kept constant does not have an effect that decreases the T_m value. In DSC analysis, there was no expected decrease in T_m value since the PVA ratio was always constant in PVA/GEL, PVA/GEL/VAN, PVA/GEL/FLU, PVA/GEL/VAN/FLU fiber wound dressing samples. On the contrary, it has been observed that drug has the effect of increasing the T_m value. The T_m value increased when the drugs were added.

3.4. Mechanical Properties of Nanofibrous Patches

The membranes used to support the functionality of tissue engineering nanofibrous patches must be able to withstand heavy loads and retain deformation.[41] The tensile strength and strain at break of three samples from each of the nanofibrous patches were examined and the results are shown in **Figure 4**. The tensile strength of pure PVA/GEL nanofibrous patch is 8.17 ± 0.21 MPa, while the strain at break has a value of 45.86 ± 2.6%. When FLU was added to these PVA/GEL nanofibrous patches, the tensile strength decreased to 6.73 ± MPa and the elongation decreased to 28.45 ± 0.4%. The addition of FLU caused a decrease in mechanical strength.[7] When VAN was added to pure PVA/GEL nanofibrous patches, the tensile strength decreased to 6.26 ± MPa and the elongation decreased to 26.8 ± 2.1%. In the study by Davani et al., they concluded that the mechanical strength of the fibers decreased when the VAN was loaded into the nanofibrous patches.[42] In addition, Zhang et al. reported that the addition of a low molecular drug VAN to nanofi-

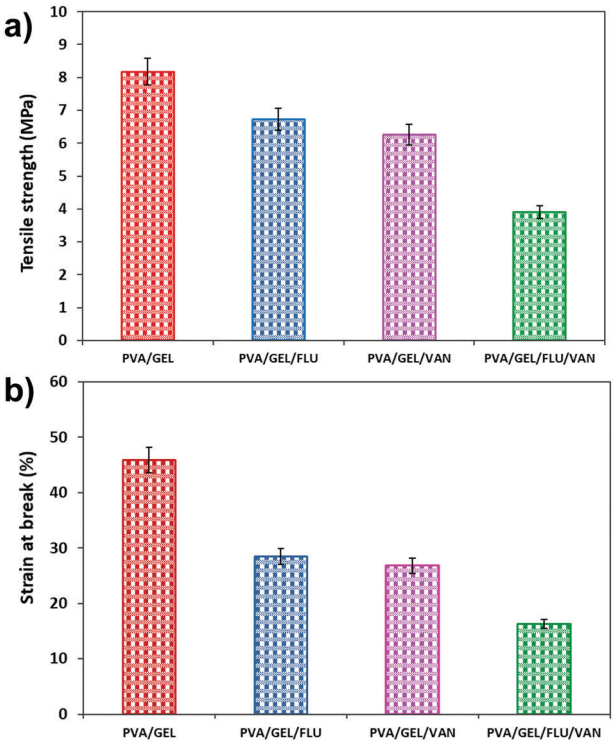

Figure 4. Tensile properties of nanofibrous patches: a) tensile strength and b) strain at break.

brous patches has a plasticizing effect on the fibers, which reduces their mechanical properties.[43] It can be seen that loading of FLU and VAN drugs separately into the PVA/GEL nanofibrous patch decreased both the tensile strength and the elongation at break. In addition, when FLU and VAN drugs were loaded together into the PVA/GEL nanofibrous patch, the tensile strength decreased to 3.9 ± 0.5 and the elongation at break to 16.28 ± 1.1%. It appears that the reduction in mechanical properties of dual loaded fibers was much huger than for individual fibers. Cam et al. observed that the mechanical properties were reduced when they loaded the drugs together into the nanofibrous patches.[44]

3.5. Swelling and Degradation

In order to estimate the release rates of the active ingredients, swelling kinetics tests are required. The natures of the polymer and the solvent have a fundamental bearing on how a polymer will swell in that solvent.[45] **Figure 5**a represents the swelling ratios of the nanofibrous patches at 37 °C. It can be observed that the PVA/GEL nanofibrous patches swell up to the 2nd day and then degradation begins. It can be observed that PVA/GEL/FLU and PVA/GEL/VAN nanofibrous patches have closer water uptake ratios, and the degradation accelerates by the 3rd day. It can also be seen that dual drug-loaded PVA/GEL/FLU/VAN nanofibrous patches show less swelling compared to other fibers. Sharma et al. reported that unloaded nanofibers had a higher degree of swelling than drug-loaded fibers as drug-loaded nanofibers have a lower absorption capacity.[46]

Degradation is the process through which structures exposed to PBS eventually degrade and lose mass.[47] Different degradation rates were observed for nanofibrous patches. As shown in Figure 5b, the PVA/GEL nanofibrous patches exhibited a higher degradation rate compared to the other nanofibrous patches. For the PVA/GEL/FLU/VAN group, nanofibrous patches start to degrade after 3rd day. All nanofibrous patches exhibited a proportional degradation rate. According to the literature, materials that absorb more water and have adequate swelling capabilities demonstrate faster weight loss.[48] When the results were examined, we observed that the degradation rate decreased when the fibers were loaded with drugs.

3.6. In vitro Drug Release Test and Drug Kinetic Studies

In this research, nanofibrous patches developed for corneal ulcers were used to conduct in vitro drug release studies to examine the release characteristics of various medications. FLU absorption value (R^2 = 0.9 986) and VAN absorption value (R^2 = 0.9 921) of drugs dissolved in solvents at different concentrations (2, 4, 6, 8, 10 μg mL^{-1}) were obtained (**Figures 6**a and **7**a). The linear standard calibration curves for the FLU and VAN were initially built by UV spectroscopy. The released FLU and VAN were detected by UV 260, 281 nm absorbance, respectively (Figures 6b and 7b). Then, to determine how much drugs were loaded into the nanofibrous patches, the encapsulation efficiency test of the nanofibrous patches was assessed. The encapsulation efficiency values were found to be 92.3% and 48.85%, respectively, for PVA/GEL/FLU and PVA/GEL/VAN nanofibrous patches (Figures 6c and 7c).

Subsequently, to determine the release kinetics of encapsulated drugs, in vitro release tests for nanofibrous patches loaded with drugs were then carried out. In order to simulate the physiological conditions of living organisms, the releasing profiles of drug-loaded nanofibrous patches were studied in phosphate-buffered saline with a pH of 7.4 and a regulated temperature of 37 °C. When the FLU release from nanofibrous patches is examined, it can be seen that although a burst release is observed in the first 6 h, the release still extends up to 96 h. It can be said that the hydrophilic feature of both drugs causes a rapid burst release, as well as the high integration into PVA/GEL nanofibrous patches, which have a water-soluble nature. It is also clear that the releases are prolonged for up to 96 h due to the cross-linking effect (Figure 6d). As shown in Figure 7d, PVA/GEL/VAN nanofibrous patch demonstrated a burst drug release in the first 12 h, which is attributed to the highly water-soluble nature of VAN. However, it took up to 96 h to complete the VAN drug release from the nanofibrous patch. Acetyl bridges between the aldehyde ends of GA and the hydroxyl groups of PVA nanofibrous patches are created when they are cross-linked with GA vapor, which lowers the solubility of the nanofibrous patches in water. All of the nanofibrous patches in this investigation were cross-linked with GA vapor for 5 h, giving all drugs a more controlled release.[49]

The release kinetics of VAN and FLU were examined using zero-order, first-order, Korsmeyer–Peppas, Higuchi, Hixon–

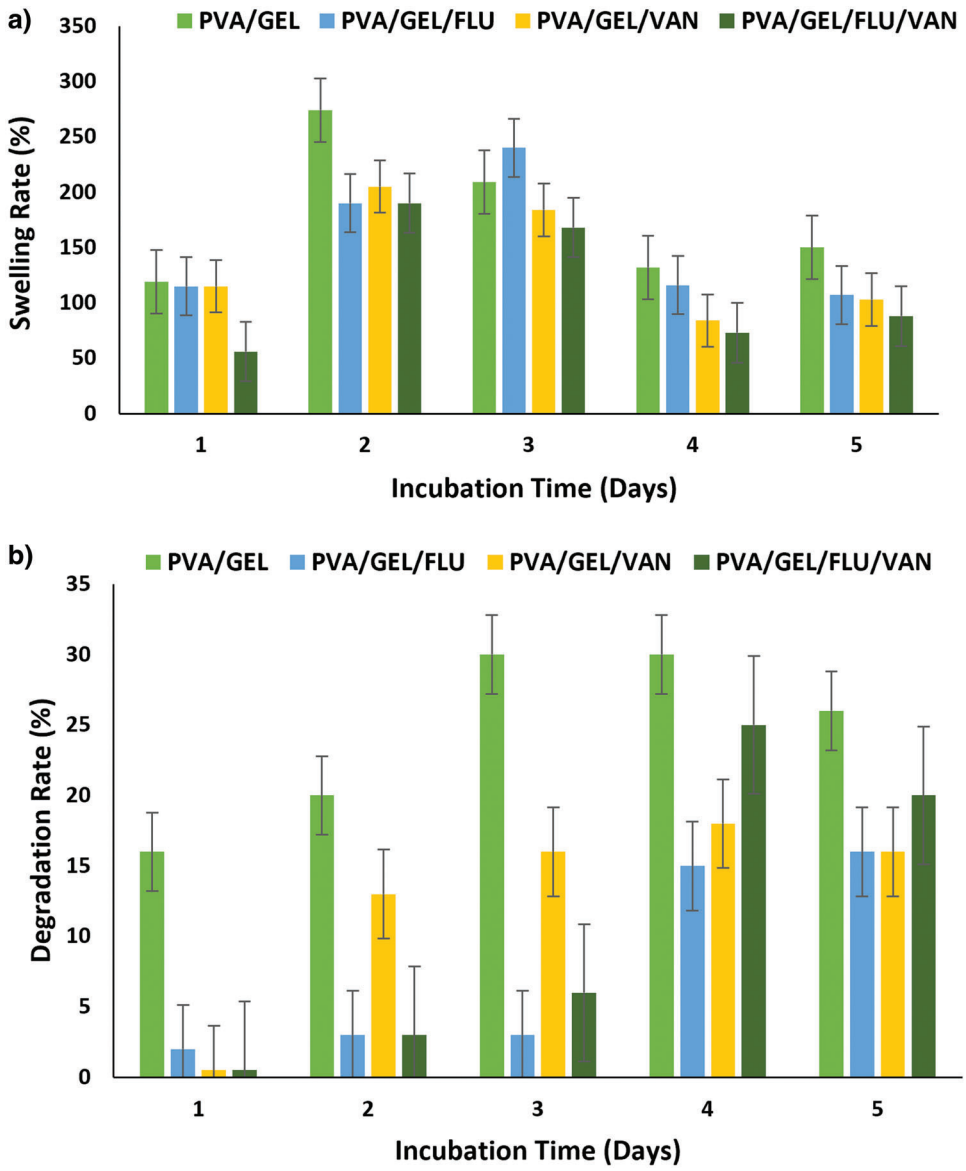

Figure 5. Swelling a) and degradation b) behaviors of nanofibrous patches.

Crowell model (**Figure 8**). The mathematical model with the highest correlation coefficient (R^2) was found to be appropriate and the kinetic constants and R^2 values of the nanofibrous patches are given in **Table 2**. According to the results obtained, it can be said that the VAN release from nanofibrous patches occurred according to the Higuchi model with the highest correlation coefficient. Higuchi is defined as the square root of a time-dependent process based on the fickian diffusion of the drug from an immediately insoluble matrix.[50] In contrast, FLU release from nanofibrous patches supports the Korsmeyer–Peppas model (Figure 8). The Korsmeyer–Peppas model relates the diffusion-dependent drug release mechanism from the polymeric material to the elapsed time.[51] In addition, the "*n*" value, which makes indicates the drug release mechanism from the polymeric material, is related to the Korsmeyer–Peppas model. The ranges of the "*n*" value in the literature are shown in **Table 3**.[48] When the "*n*" values were evaluated, both drugs exhibited a Super-Case-II release mechanism according to the Korsmeyer–Peppas model. Super Case-II represents the release mechanism of hydrophilic polymer swelling in water and biological fluids as a result of chain relaxation.[52]

3.7. Antifungal and Antibacterial Effects of FLU and VAN-Loaded PVA/GEL Nanofibrous Patches

The antifungal effects of PVA/GEL nanofibrous patches loaded with FLU alone and in combination with VAN were assessed by the disc diffusion method using *C. albicans*. **Figure 9** and **Table 4** show the zone of inhibition formed by PVA/GEL/FLU and PVA/GEL/FLU/VAN nanofibrous patches. PVA/GEL/FLU nanofibrous patches showed inhibition zone with diameter of

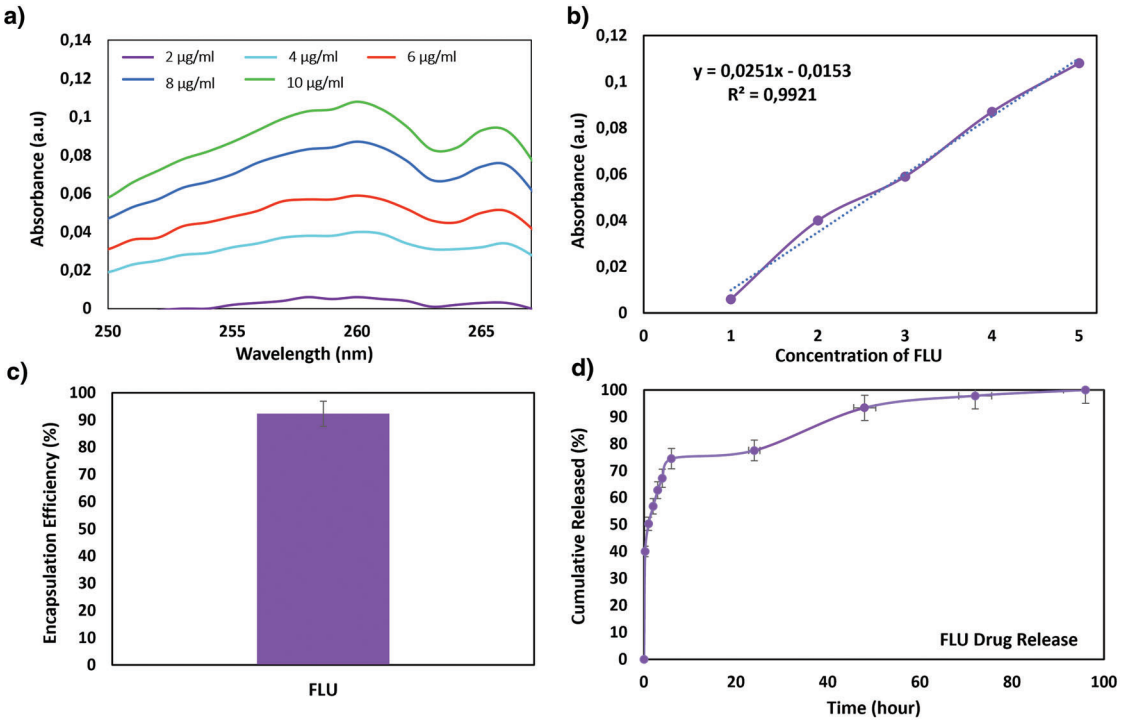

Figure 6. In vitro drug release profiles of PVA/GEL/FLU nanofibrous patch: Absorption spectra of FLU at different concentrations a), FLU calibration curve b), encapsulation efficiency of PVA/GEL/FLU nanofibrous patch c), drug release profiles from the PVA/GEL/FLU nanofibrous patch d). All the measurements were repeated three times, and the errors were less than 5%.

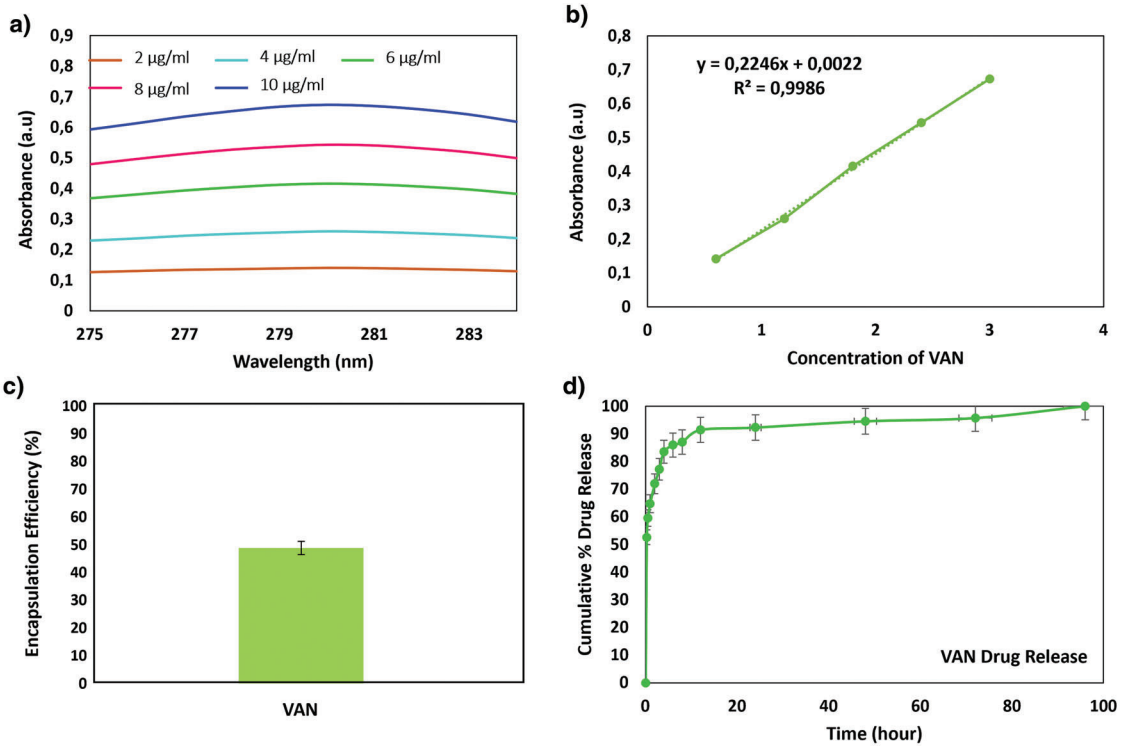

Figure 7. In vitro drug release profiles of PVA/GEL/VAN nanofibrous patch: Absorption spectra of VAN at different concentrations a), VAN calibration curve b), encapsulation efficiency of PVA/GEL/VAN nanofibrous patch c), drug release profiles from the PVA/GEL/VAN nanofibrous patch d). All the measurements were repeated three times, and the errors were less than 5%.

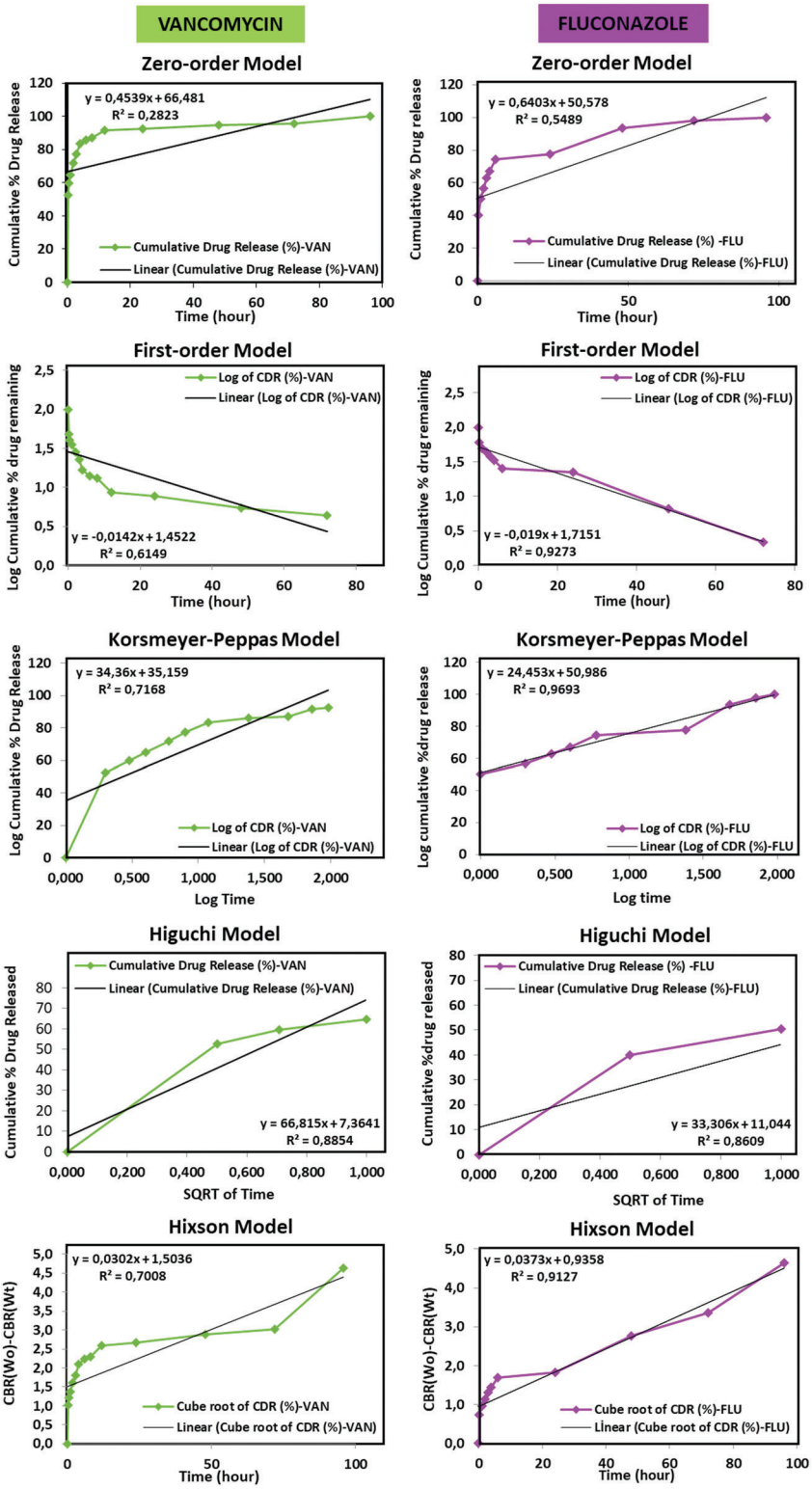

Figure 8. Zero-order, first-order, Korsmeyer–Peppas, Higuchi, and Hixson–Crowell kinetic release patterns of FLU and VAN drug release profiles.

Table 2. Results of mathematical drug release patterns of nanofibrous patches.

	Korsmeyer–Peppas		Zero-Order		First-Order		Higuchi		Hixson–Crowell	
Sample	R^2	n	R^2	K_0	R^2	K_1	R^2	K_h	R^2	K_{hc}
PVA/GEL/FLU	24.453	36.356	0.5489	0.6403	0.9273	−0.019	0.8609	33.30	0.9127	0.0373
PVA/GEL/VAN	34.36	37.957	0.2823	0.4539	0.6149	−0.0142	66.815	13.877	0.0302	0.0208

Table 3. Transport mechanisms where the "n" value corresponds.

The ranges of n values	Transport mechanisms
$0.45 \leq n$	Fickian diffusion mechanism
$0.45 < n < 0.89$	Non-Fickian transport
$n = 0.89$	Case II (relaxational) transport
$n > 0.89$	Super case II transport

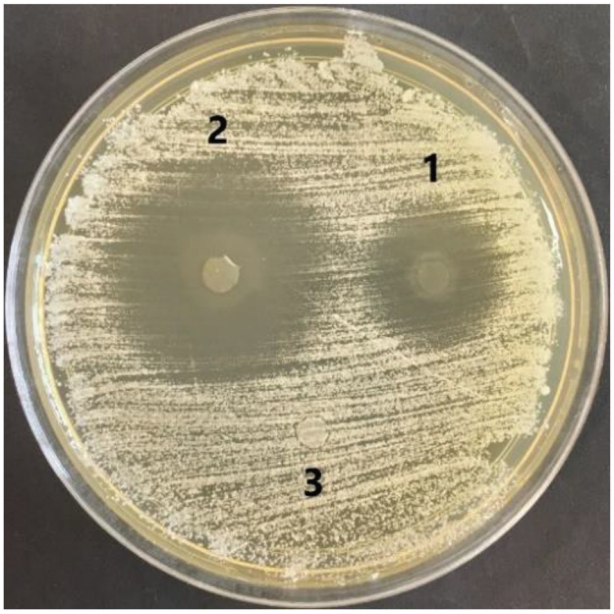

Figure 9. The antifungal effect of FLU and VAN loaded PVA/GEL nanofibrous patches against *C. albicans* 1) FLU loaded PVA/GEL nanofibrous patch, 2) FLU and VAN loaded PVA/GEL nanofibrous patch, 3) blank PVA/GEL nanofibrous patch (negative control).

Table 4. The diameter of the inhibition zones around the nanofibrous patches.

	Zone of inhibition (mean diameter [mm])		
	PVA/GEL/FLU	PVA/GEL/FLU/VAN	PVA/GEL(control)
C. albicans	20 mm	30 mm	—
	PVA/GEL/VAN	PVA/GEL/FLU/VAN	PVA/GEL(control)
S. aureus	8 mm	12 mm	—

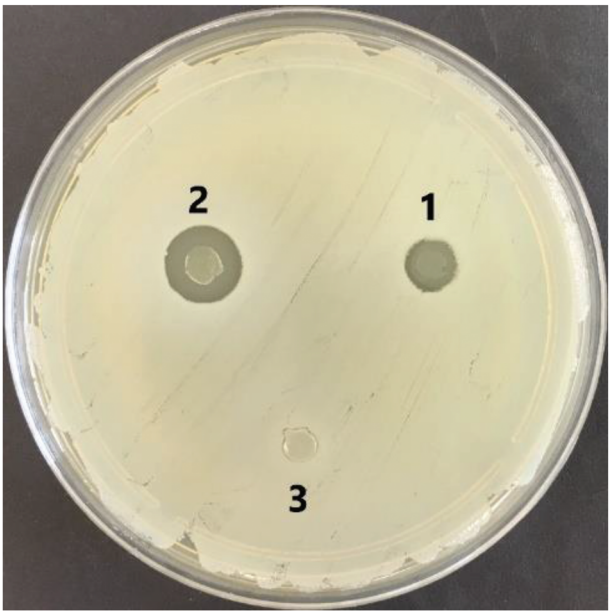

Figure 10. The antibacterial effect of PVA/GEL nanofibrous patches against *S. aureus* 1) PVA/GEL/VAN nanofibrous patch, 2) loaded PVA/GEL/FLU/VAN nanofibrous patch, 3) blank PVA/GEL nanofibrous patch (negative control).

20 mm, while PVA/GEL/FLU/VAN nanofibrous patch showed 30 mm inhibition zone. This result suggests that VAN increased the activity of FLU against *C. albicans* when drugs were used in combination (Figure 9). Our results of the disc diffusion assay are consistent with previous studies that have reported that the combination of FLU with nonantifungal agents such as antibacterials enhanced its effectiveness.[48] Ku et al. screened several antibiotics including azithromycin and tigecycline (TIG) against *C. albicans* and demonstrated that tigecycline increased the antifungal effect of FLU against *C. albicans* biofilms.[53,54] The antibacterial activity of PVA/GEL/VAN and PVA/GEL/FLU/VAN nanofibrous patches was also evaluated. **Figure 10** and Table 4 show the effect of PVA/GEL/VAN and PVA/GEL/FLU/VAN nanofibrous patches against *S. aureus*. As seen in Figure 10, fibers loaded with combination of FLU and VAN exhibited better antibacterial activity. The blank PVA/GEL fibers used as negative control had no antibacterial effect. The antibacterial activity of VAN loaded nanofibrous patches has been studied earlier. Heba et al. reported the antibacterial activity of VAN loaded ALG-based nanofibrous patches produced by the electrospinning method.[55]

Overall, our results indicated that PVA/GEL/FLU, PVA/GEL/VAN, and PVA/GEL/FLU/VAN nanofibrous patches have significant antifungal and antibacterial activities and could be great carriers for antimicrobial agent delivery in corneal infections.

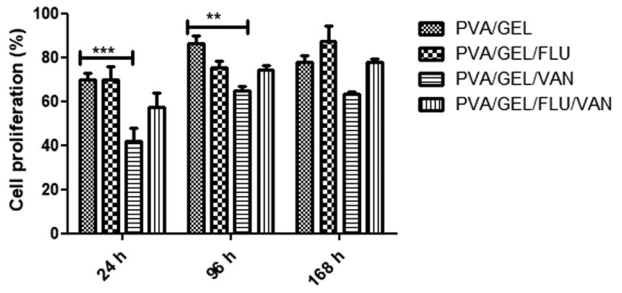

Figure 11. Cell proliferation percentage of NIH3T3 cells on PVA/GEL, PVA/GEL-FLU, PVA/GEL-VAN, and PVA/GEL-FLU-VAN nanofibrous patches on the 1st, 4th, and 7th days (***$p < 0.001$ and $p < 0,01$ vs PVA/GEL).

3.8. Biocompatibility and Functional Features of Nanofibrous Patches

Figure 11 shows the results of MTT assay after 24, 96, and 168 h compared to control. It was observed that PVA/GEL/VAN and PVA/GEL/FLU/VAN nanofibrous patches exhibited the lowest viability of cells after 24 h ($p < 0.001$). We can attribute this effect to the burst releasing effect of VAN, which caused temporary suppression of the proliferation. As a matter of fact, after 96 h, it can be seen in Figure 11 that cells cultured with the PVA/GEL-FLU-VAN nanofibrous patch increased the proliferation after 168 h, while cells cultured on PVA/GEL/VAN exhibited much lower poliferation rate. PVA/GEL/VAN nanofibrous patch continues ($p < 0.01$). After 168 h, it was determined that the proliferation of cells on the PVA/GEL, PVA/GEL/FLU, and PVA/GEL/FLU/VAN gradually increased ($p > 0.05$).

In agreement with proliferation studies, SEM images showed expansion and growth of cells on the PVA-based nanofibrous patches. Although these images indicated that fibroblast cells were successfully adhered to nanofibrous patches, there was a considerable difference in cell morphology depending on the surface structure and chemistry (**Figure 12**). NIH3T3 cells that were cultured on PVA/GEL/FLU/VAN nanofibrous patch spread in many directions and appeared much more mature and flattened in comparison with those adhered to PVA/GEL/FLU and PVA/GEL/VAN.

DAPI staining also showed more NIH3T3 cells attached to the PVA/GEL/FLU and PVA/GEL/FLU/VAN nanofibrous patches. **Figure 13** showed that only a small population of NIH3T3 cells were adhered on PVA/GEL/VAN nanofibrous patch.

Electrospun nanofibrous patches are considered as ideal wound dressings due to their high surface area/volume ratio, controlled drug or biomolecule release, and flexibility. For this reason, electrospun nanofibrous patches obtained by different electrospinning methods are widely used in wound healing applications.[56,57] In our study, the in vitro wound healing properties of PVA/GEL based nanofibrous patches were also investigated. It was observed that the wound healing properties of PVA/GEL/FLU and PVA/GEL/FLU/VAN nanofibrous patches were more pronounced than PVA/GEL/VAN at the end of 48 h (**Figure 14**).

Some of the most important functional features of the investigated nanofibrous corneal patches, like the contact angle, the refractive index, and the oxygen permeability, needs to be discussed. All the mentioned features may notably affect the patient's comfort and safety of the utilization of the nanofibrous patches.

The contact angle (CA) could help evaluate the ability of the patches to keep a stable tear film within the ocular surface.[58] It is worth mentioning that the contact angle of the nanofibrous patch made of the investigated blend 13% PVA/0.5% GEL was earlier determined.[28] The measured value of CA was 32.6° ± 1.1°. By adding 3% drug (propolis) into the composition, the contact angle becomes 26.4° ± 1.5° indicating that propolis addition decreased the contact angle of the PVA/GEL blend. Contact angles of the most popular types of silicone lenses (available at the time of the mentioned study) were measured, and they ranged

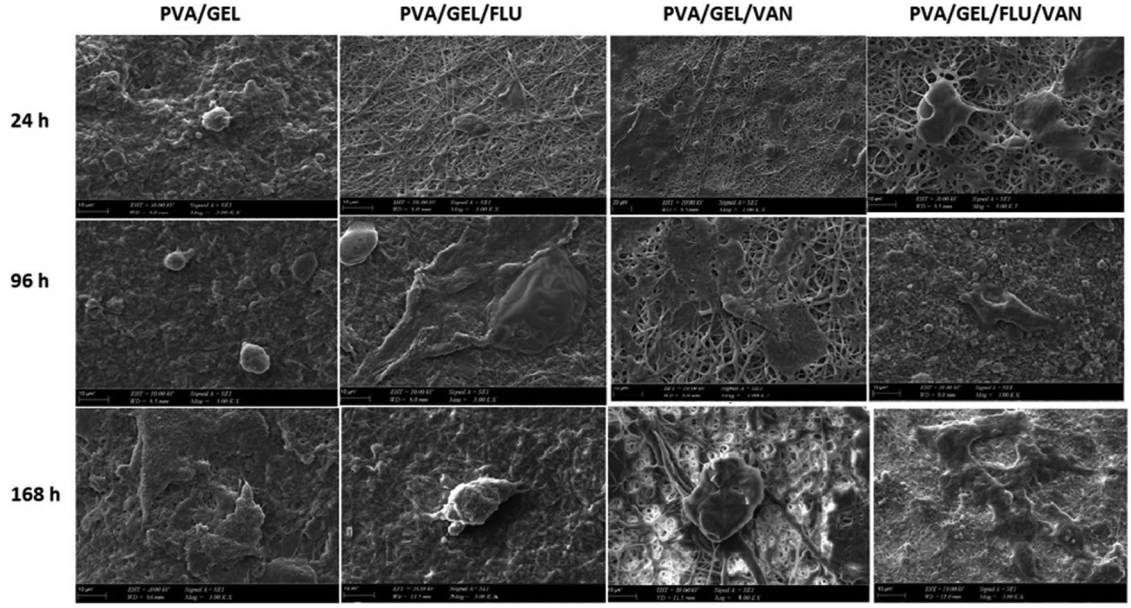

Figure 12. SEM images showing the NIH3T3 cell morphology on nanofibrous patches (scale bar = 10 μm) at the 1st, 4th, and 7th days.

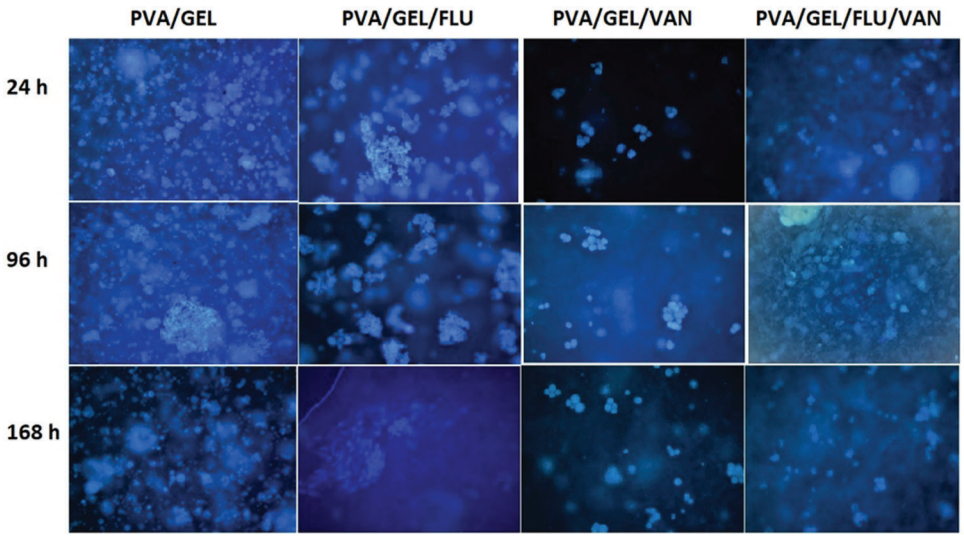

Figure 13. 8. Microscopic images of DAPI-stained cells at 24, 96, and 168 h of culturing in contact with PVA/GEL, PVA/GEL-FLU, PVA/GEL-VAN, and PVA/GEL-FLU-VAN nanofibrous patches at 20 × objective magnification.

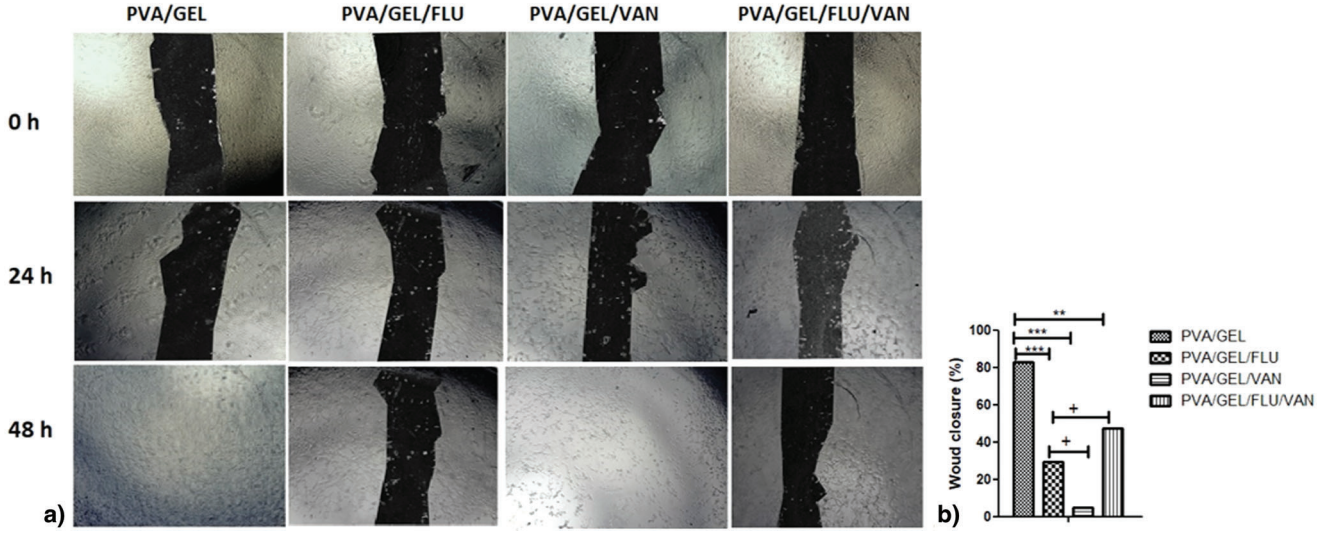

Figure 14. a) Representative micrographs of in vitro wound healing activity of nanofibrous patches. b) Quantification of wound closure at 48 h on PVA/GEL-based dual drug loaded nanofibrous patches. $^{***}p < .001$, $^{**}p < 0.01$ versus PVA/GEL and $p < 0.05$ versus PVA/GEL-FLU-VAN.

broadly from 43° to 93°.[59] Considering the relatively low CA of drug-free PVA/GEL patches, one can assume that all the investigated nanofibrous patches are promising to offer proper wettability.

The refractive index (RI) of any corneal dressing material is an important physical parameter that affects visual acuity. For most of the hydrogel materials, the RI is closely correlated with the water content.[60] The RI of the investigated nanofibrous patches n_{patch} could be estimated based on the Gladstone–Dale equation[61]

$$n_{patch} = \sum n_i v_i \quad (10)$$

where n_i represents the refractive indices, and v_i the volume fractions of the individual components. One can predict the resultant refractive index of the corneal patch using the refractive indices of all the patch components.[62] It is worth emphasizing that the PVA/GEL nanofibrous patch in the swollen state is characterized by high water content, which can reach up to 87%,[63] and, therefore, cannot be ignored during RI calculations. The RI of water is 1.33,[62] whereas the RI of PVA ranges between 1.5[64] and 1.6.[65] Ignoring the effect of gelatin, the RI of swollen PVA/GEL nanofibrous patches was estimated as 1.39. The determined value is in accordance with the relationship between the RI and the water content identified for different conventional hydrogel soft contact lens materials. It is worth mentioning that the water content of

conventional hydrogel (without silicone) soft contact lens usually do not exceed 75%.[66]

The oxygen permeability is a notable functional feature characterizing the investigated nanofibrous patches since the corneal dressing materials should ensure proper oxygen supply to the cornea. The oxygen permeability is indicated as *Dk*, where *D* is the diffusivity and *k* is the solubility (a measure of how much oxygen is contained in the material).[58] The oxygen permeability of the investigated nanofibrous patches could be estimated since hydrated PVA/GEL blends could be classified as conventional hydrogel materials (nonsilicon hydrogels).[58] Hydrogels transport oxygen via the water channels, and their oxygen permeability is closely related to the water content *W*, according to the following equation[35]

$$Dk = 1.67e^{0.0397W} \tag{11}$$

In the swollen state, the PVA/GEL nanofibrous patch has a relatively high-water content of 87%.[63] The estimated *Dk* of investigated PVA/GEL nanofibrous patches is 52, which is comparable with the oxygen permeability of some of the most popular types of modern silicone lenses.[58]

4. Conclusions

In this study, antibiotic and antifungal dual-drug loaded dual-layered PVA/GEL nanofibrous patches were produced by electrospinning as an alternative treatment of corneal ulcers. Antifungal agent FLU and antibacterial agent VAN were included in PVA/GEL nanofibrous patches to suppress *C. albicans* and *S. aureus* that cause corneal ulcers. FT-IR and DSC studies demonstrated full incorporation of the drugs into PVA/GEL nanofibrous patches. SEM images showed that nanofibrous patches with no beads and smooth surfaces were obtained in both pure and drug-loaded nanofibrous patches. Their addition of the drugs caused an increase in nanofibrous patches diameters. The tensile test results reported that loading the FLU and VAN drugs separately on the PVA/GEL nanofibrous patch decreased both the tensile strength and elongation at break, while it was further reduced when combining two drug-loaded layers in one patch. When the drug release results were analyzed, the FLU and VAN-loaded nanofibrous patches showed a controlled release profile extending up to 96 h. The successful release of FLU and VAN was further confirmed by the antimicrobial tests. The in vitro antimicrobial tests showed that FLU and VAN loaded PVA/GEL nanofibrous patches exhibited significant antifungal and antibacterial activities against *C. albicans* and *S. aureus* and are promising candidates to be used as potential tools for the treatment of corneal ulcers. The cytocompatibility of PVA/GEL based nanofibrous patches also was investigated MTT assay, DAPI staining, SEM and, wound healing assay. Results from these studies showed that PVA/GEL/FLU and PVA/GEL/FLU/VAN nanofibrous patches can provide a suitable substrate for cells to settle and grow. The novelty of this study is to develop a potential rapid treatment modality for the treatment of corneal ulcers of aggressive nature with dual drug therapy.

Acknowledgements

This study was performed in the frame of bilateral Polish–Turkish project – CorPatch – financially supported by TUBITAK (Project. No. 120N333) and the National Centre for Research and Development (Contract No. POLTUR4/CorPatch/1/2021). In addition, it was performed in the frame of the Marmara University Scientific Research Committee (Project No. FDK-2021-10345). E.I. is a YOK 100/2000 doctoral fellow in this research.

Conflict of Interest

The authors declare no conflict of interest.

Data Availability Statement

The data that support the findings of this study are available from the corresponding author upon reasonable request.

Keywords

corneal tissue engineering, corneal ulcers, electrospinning, fluconazole, vancomycin

Received: December 23, 2022
Revised: February 26, 2023
Published online:

[1] K. M. Meek, C. Knupp, *Prog. Retinal Eye Res.* **2015**, *49*, 1.
[2] C. E. Willoughby, D. Ponzin, S. Ferrari, A. Lobo, K. Landau, Y. Omidi, *Clin. Exp. Ophthalmol.* **2010**, *38*, 2.
[3] M. S. Insler, G. Boutros, D. W. Boulware, *Am. Intra-Ocul. Implant Soc. J.* **1985**, *11*, 594.
[4] S. S. Tuli, G. S. Schultz, D. M. Downer, *Ocul. Surf.* **2007**, *5*, 23.
[5] L. B. Byrd, N. Martin, *Corneal Ulcer*. In: StatPearls [Internet]. StatPearls Publishing, Treasure Island (FL) **2023**, 30969511.
[6] Y. Gong, W. Liu, X. Huang, L. Hao, L. Y. Sun, *Front. Microbiol.* **2019**, *10*, 1461.
[7] E. Ilhan, S. Cesur, R. B. Sulutas, E. Pilavci, B. Dalbayrak, E. Kaya, E. D. Arisan, G. B. Tinaz, M. Sengor, E. Kijeńska-Gawrońska, F. N. Oktar, O. Gunduz, *Eur. Polym. J.* **2022**, *176*, 111390.
[8] D. Guimarães, A. Cavaco-Paulo, E. Nogueira, *Int. J. Pharm.* **2021**, *601*, 120571.
[9] P. Yehgambaram, R. G. S. V. Prasad, V. S. Jakka, R. S. L. Aparna, A. R. Phani, *J. Pharm. Res.* **2013**, *6*, 26.
[10] R. Sharma, T. Garg, A. K. Goyal, G. Rath, *Artif. Cells, Nanomed., Biotechnol.* **2016**, *44*, 524.
[11] M. Gupta, M. L. Durand, L. Sobrin, *Int. Ophthalmol. Clin.* **2011**, *51*, 167.
[12] C. A. García-González, J. Barros, A. Rey-Rico, P. Redondo, J. L. Gómez-Amoza, A. Concheiro, C. Alvarez-Lorenzo, F. J. Monteiro, *ACS Appl. Mater. Interfaces* **2018**, *10*, 3349.
[13] B. S. Kotlus, R. A. Wymbs, E. M. Vellozzi, I. J. Udell, *Am. J. Ophthalmol.* **2006**, *142*, 726.
[14] M. Naeimi, R. Tajedin, F. Farahmandfar, M. Naeimi, M. Monajjemi, *Mater. Res. Express* **2020**, *7*, 095401.
[15] Y. Sun, P. Zhang, F. Zhang, M. Pu, W. Zhong, Y. Zhang, Y. Shen, B. Zuo, *J. Drug Delivery Sci. Technol.* **2022**, *75*, 103596.
[16] A. K. Riau, D. Mondal, T. T. Aung, E. Murugan, L. Chen, N. C. Lwin, L. Zhou, R. W. Beuerman, B. Liedberg, S. S. Venkatraman, J. S. Mehta, *ACS Biomater. Sci. Eng.* **2015**, *1*, 1324.
[17] Y. Zhao, C. Tian, K. Wu, X. Zhou, K. Feng, Z. Li, Z. Wang, X. Han, *Front. Bioeng. Biotechnol.* **2021**, *9*, 760395.

[18] L. Éva Uhljar, S. Yuan Kan, N. Radacsi, V. Koutsos, P. Szabó-Révész, R. Ambrus, M. Popa, *Pharmaceutics* **2021**, *13*, 556.
[19] H. Izgis, E. Ilhan, C. Kalkandelen, E. Celen, M. M. Guncu, H. Turkoglu Sasmazel, O. Gunduz, D. Ficai, A. Ficai, G. Constantinescu, *Nanomaterials* **2022**, *12*, 3040.
[20] A. Luraghi, F. Peri, L. Moroni, *J. Controlled Release* **2021**, *334*, 463.
[21] S. Cesur, F. N. Oktar, N. Ekren, O. Kilic, D. B. Alkaya, S. A. Seyhan, Z. R. Ege, C.-C. Lin, S. E. Kuruca, G. Erdemir, O. Gunduz, *J. Australas. Ceram. Soc.* **2019**, *56*, 533.
[22] S. A. Seyhan, D. B. Alkaya, S. Cesur, F. N. Oktar, O. Gunduz, *J. Australas. Ceram. Soc.* **2022**, *58*, 1231.
[23] T. A. Tut, S. Cesur, E. Ilhan, A. Sahin, O. S. Yildirim, O. Gunduz, *Eur. Polym. J.* **2022**, *179*, 111580.
[24] S. Cesur, M. E. Cam, F. S. Sayın, S. Su, A. Harker, M. Edirisinghe, O. Gunduz, *Langmuir* **2021**, *38*, 5040.
[25] H. Miyashita, S. Shimmura, H. Kobayashi, T. Taguchi, N. Asano-Kato, Y. Uchino, M. Kato, J. Shimazaki, J. Tanaka, K. Tsubota, *J. Biomed. Mater. Res., Part B* **2006**, *76*, 56.
[26] D. Jain, E. Carvalho, A. K. Banthia, R. Banerjee, *Drug Dev. Ind. Pharm.* **2011**, *37*, 167.
[27] C.-Y. Huang, K.-H. Hu, Z.-H. Wei, *Sci. Rep.* **2016**, *6*, 37960.
[28] S. Ulag, E. Ilhan, R. Demirhan, A. Sahin, B. K. Yilmaz, B. Aksu, M. Sengor, D. Ficai, A. M. Titu, A. Ficai, O. Gunduz, *Molecules* **2021**, *26*, 2577.
[29] E. Ilhan, Z. Karahaliloglu, E. Kilicay, B. Hazer, E. B. Denkbas, *Mater. Technol.* **2020**, *35*, 179.
[30] E. Ilhan, S. Ulag, A. Sahin, N. Ekren, O. Kilic, F. N. Oktar, O. Gunduz, *Lect. Notes Bioinf.* **2020**, *12108*, 175.
[31] S. Yang, X. Zhang, D. Zhang, *Int. J. Mol. Sci.* **2019**, *20*, 4395.
[32] D. Semnani, M. Afrashi, F. Alihosseini, P. Dehghan, M. Maherolnaghsh, *J. Mater. Sci.: Mater. Med.* **2017**, *28*, 175.
[33] F. Kalalinia, Z. Taherzadeh, N. Jirofti, N. Amiri, N. Foroghinia, M. Beheshti, B. S. F. Bazzaz, M. Hashemi, A. Shahroodi, E. Pishavar, S. A. S. Tabassi, J. Movaffagh, *Int. J. Biol. Macromol.* **2021**, *177*, 100.
[34] J. Ruiz-Alcocer, D. Monsálvez-Romín, S. García-Lázaro, C. Albarrán-Diego, J. L. Hernández-Verdejo, D. Madrid-Costa, *Clin. Exp. Optom.* **2018**, *101*, 188.
[35] P. B. Morgan, N. Efron, *Contact Lens Anterior Eye* **1998**, *21*, 2.
[36] S. Cesur, M. E. Cam, F. S. Sayin, O. Gunduz, *J. Drug Delivery Sci. Technol.* **2022**, *67*, 102977.
[37] N. Indora, D. Kaushik, *Int. J. Eng. Sci. Invent. Res. Dev.* **2015**, *I*, 280.
[38] M. Ghosh, S. Mandal, A. Roy, S. Chakrabarty, G. Chakrabarti, S. K. Pradhan, *Mater. Sci. Eng., C* **2020**, *106*, 110160.
[39] S. Ulag, A. Sahin, M. M. Guncu, B. Aksu, N. Ekren, M. Sengor, D. M. Kalaskar, O. B Gunduz, *Bioprinting* **2021**, *24*, e00173.
[40] N. T. B. Linh, Y. K. Min, H. Y. Song, B. T. Lee, *J. Biomed. Mater. Res., Part B* **2010**, *95*, 184.
[41] H. R. Bakhsheshi-Rad, Z. Hadisi, A. F. Ismail, M. Aziz, M. Akbari, F. Berto, X. B. Chen, *Polym. Test.* **2020**, *82*, 106298.
[42] F. Davani, M. Alishahi, M. Sabzi, M. Khorram, A. Arastehfar, K. Zomorodian, *Mater. Sci. Eng., C* **2021**, *123*, 111975.
[43] M. Zhang, Z. Li, L. Liu, Z. Sun, W. Ma, Z. Zhang, R. Zhang, D. Sun, *J. Nanomater.* **2016**, *2016*, 9159364.
[44] M. E. Cam, B. Ertas, H. Alenezi, A. N. Hazar-Yavuz, S. Cesur, G. S. Ozcan, C. Ekentok, E. Guler, C. Katsakouli, Z. Demirbas, D. Akakin, M. S. Eroglu, L. Kabasakal, O. Gunduz, M. Edirisinghe, *Mater. Sci. Eng., C* **2021**, *119*, 111586.
[45] D. J. Buckley, M. Berger, D. Poller, *J. Polym. Sci.* **1962**, *56*, 163.
[46] A. Sharma, A. Gupta, G. Rath, A. Goyal, R. B. Mathur, S. R. Dhakate, *J. Mater. Chem. B* **2013**, *1*, 3410.
[47] E. Ilhan, S. Cesur, E. Guler, F. Topal, D. Albayrak, M. M. Guncu, M. E. Cam, T. Taskin, H. T. Sasmazel, B. Aksu, F. N. Oktar, O. Gunduz, *Int. J. Biol. Macromol.* **2020**, *161*, 1040.
[48] E. Saylam, Y. Akkaya, E. Ilhan, S. Cesur, E. Guler, A. Sahin, E. Cam, N. Ekren, F. Nuzhet Oktar, O. Gunduz, D. Ficai, A. Ficai, P. Calandra, D. Lombardo, *Appl. Sci.* **2021**, *11*, 10727.
[49] Z. Cui, Z. Zheng, L. Lin, J. Si, Q. Wang, X. Peng, W. Chen, *Adv. Polym. Technol.* **2018**, *37*, 1917.
[50] M. Singh, S. Pilani, *Int. J. Pharm. Stud. Res.* **2021**, *2*, 77.
[51] M. Kalam, M. Humayun, N. Parvez, S. Yadav, *Egypt. Pharm. Bull.* **2007**, *1*, 30.
[52] D. Solanki, M. Motiwale, *Int. J. ChemTech Res.* **2020**, *13*, 166.
[53] S. Liu, Y. Hou, X. Chen, Y. Gao, H. Li, S. Sun, *Int. J. Antimicrob. Agents* **2014**, *43*, 395.
[54] T. S. N. Ku, S. K. A. Palanisamy, S. A. Lee, *Int. J. Antimicrob. Agents* **2010**, *36*, 441.
[55] H. A. Fathi, A. Abdelkader, M. S. AbdelKarim, A. A. Abdelaziz, M. A. El-Mokhtar, A. Allam, G. Fetih, M. El Badry, M. Elsabahy, *Int. J. Pharm.* **2020**, *586*, 119620.
[56] V. K. Thakur, M. K. Thakur, *Eco-Friendly Polymer Nanocomposites: Chemistry and Applications*, *Vol. 74*, Springer, New York **2015**.
[57] H. Chen, Y. Peng, S. Wu, L. P. Tan, *Materials* **2016**, *9*, 272.
[58] R. Moreddu, D. Vigolo, A. K. Yetisen, *Adv. Healthcare Mater.* **2019**, *8*, 1900368.
[59] C. Maldonado-Codina, P. B. Morgan, *J. Biomed. Mater. Res., Part A* **2007**, *83A*, 496.
[60] E. Kim, K. Ehrmann, *Contact Lens Anterior Eye* **2020**, *43*, 123.
[61] J. H. Gladstone, T. P. Dale, *Proc. R. Soc. London* **1997**, *12*, 448.
[62] M. Himmler, D. W. Schubert, T. A. Fuchsluger, *Nanomaterials* **2021**, *11*, 3191.
[63] T. Ren, J. Gan, L. Zhou, H. Chen, *Polymers* **2020**, *12*, 1729.
[64] T. E. Somesh, M. Q. A. Al-Gunaid, B. S. Madhukar, Siddaramaiah, *J. Mater. Sci.* **2019**, *30*, 37.
[65] S. Mahendia, A. Kumar Tomar, P. K. Goyal, S. Kumar, *J. Appl. Phys.* **2013**, *113*, 73103.
[66] J. M. González-Méijome, M. Lira, A. López-Alemany, J. B. Almeida, M. A. Parafita, M. F. Refojo, *Ophthalmic Physiol. Opt.* **2006**, *26*, 57.